JOURNAL OF MATERIALS SCIENCE **34** (1999) 4783–4791

# High temperature creep in a 2-3-4 garnet: $Ca_3Ga_2Ge_3O_{12}$

V. VOEGELÉ*, B. LIU‡¶, P. CORDIER*, Z. WANG‡**, H. TAKEI§, P. PAN§, S. KARATO‡
*Université des Science et Technologies de Lille, L.S.P.E.S. ESA 8008, Bat. C6
59655 Villeneuve D'Ascq Cedex, France
‡University of Minnesota, Department of Geology and Geophysics, Minneapolis, MN 55455, USA
§Osaka University, Department of Engineering, Toyonaka, Osaka, Japan
¶University of Minnesota, Biomedical Engineering Institute, Minneapolis, 55455, USA
**Université de Montreal, Départment de Géologie, Montreal, H3C 3J7, Canada
E-mail: "Patrick.Cordier@univ-lille1.fr"

High temperature plastic deformation in a single crystal of a 2-3-4 garnet, $Ca_3Ga_2Ge_3O_{12}$, was investigated. A Czochralski-grown single crystal of $Ca_3Ga_2Ge_3O_{12}$ was deformed in compression in air along ⟨100⟩ or ⟨110⟩ at temperatures of 1472 to 1573 K ($T/T_m = 0.90$–$0.96$). The samples show higher resistance to creep than other 3-3 garnets, namely the flow stress at the strain-rate of $4 \times 10^{-6}$ $s^{-1}$ is ∼200–400 MPa in this temperature range. The TEM observations of dislocation microstructures show little evidence of climb and plastic deformation in this garnet appears to occur exclusively by dislocation glide, using mostly the 1/2⟨111⟩{110} slip systems. Dislocations with $\mathbf{b} = \langle 100\rangle$ are frequently observed but they are interpreted as products of dislocation reactions among 1/2⟨111⟩. The single crystal used contained a number of precipitates that grew during annealing and also during deformation. These precipitates act as sources for dislocations but no evidence for their significant effects on creep strength is observed. The normalized flow law of $Ca_3Ga_2Ge_3O_{12}$ is similar to other 3-3 oxide garnets (e.g., YAG, GGG), but in contrast to 3-3 garnets, the more stable and hence less mobile dislocations have a large edge component.

## 1. Introduction

Garnets in general have high resistance for plastic flow even at high temperatures and their mechanical properties are of interest to many engineering applications [1]. Mechanical properties of garnets are also of interest from the point of view of Earth science, because a large amount of garnets is believed to occur in the deep interior of the Earth [2, 3]. The general chemical formula for a garnet is $X_3Y_2Z_3O_{12}$ where X, Y, and Z are cations. In oxide garnets such as $Y_3Al_5O_{12}$ all the cations have 3+ charges (we will refer to them as 3-3 garnets). On the other hand, alumino-silicate garnets such as pyrope ($Mg_3Al_2Si_3O_{12}$) have cation charges of 2+, 3+ and 4+ respectively (hereafter referred to as 2-3-4 garnets). Previous studies on plastic flow of garnets were mostly concerned with oxide garnets. Karato *et al.* [4] also investigated 2-3-4 alumino-silicate garnets, but due to the difficulties in finding high quality single crystals that are stable at easily attainable conditions, understanding of mechanical properties and microscopic processes of deformation in 2-3-4 garnets has been limited.

Rabier *et al.* [5] studied the dislocation structure of garnets and suggested that electrostatic energy may play an important role in controlling the nature of stacking fault and resultant partial dislocations. They proposed that two different types of stacking fault might occur in garnet structure: electrostatic fault (EF) with the displacement vector of 1/4⟨111⟩ and order fault (OF) with the displacement vector of 1/2⟨100⟩. The order fault is associated with the modification of X and Z sublattices and, in 3-3 garnets, is not associated with any changes in electrostatic energy. On the other hand, the electrostatic fault is associated with the atomic rearrangement involving filling initially unoccupied cation sites with some cations. Therefore this latter defect involves change in electrostatic energy and is usually less favoured than the order fault. However, the situation might be different in 2-3-4 garnets where the modification of X and Z sublattices does involve a change in electrostatic energy in contrast to 3-3 garnets. Such a difference could result in a difference in the mobility of the 1/2⟨111⟩ dislocations compared to those of ⟨100⟩ dislocations [5], leading to possible differences in plastic deformation behaviour between 2-3-4 garnets and 3-3 garnets.

Therefore it seems that deformation mechanisms in 2-3-4 garnets might be different from those of 3-3 garnets, but the details have been poorly understood due to the difficulties in conducting well-defined deformation experiments on 2-3-4 garnets. To investigate the mechanisms of plastic deformation in a 2-3-4 garnet, we used synthetic single crystal of $Ca_3Ga_2Ge_3O_{12}$ garnet that is stable under a wide range of thermodynamic conditions. In addition to determining flow laws, we have conducted a detailed study of microstructures using TEM (transmission electron microscopy). This paper describes the results and discusses the microscopic mechanisms of deformation.

## 2. Experimental method

A single crystal of Czochralski-grown $Ca_3Ga_2Ge_3O_{12}$ was used in this study. The details of the growth procedure have been described elsewhere [6]. Optical grade reagents of $CaCO_3$, $Ga_2O_3$ and $GeO_2$ were mixed and precalcined at 1473 K for 40 h in air. The calcined powder was charged in a 1 mm thick Pt crucible 30 mm in diameter and 35 mm in height, and melted at about 1673 K with a 40 kW rf-heating system. The crystal growth conditions were fixed as follows: the pulling rate was 2–4 mm/h, and the rotation rate was 40 rpm. A pressurised oxygen atmosphere up to 1.2 atm was used in order to prevent the evaporation of $GeO_2$ from the melt.

The crystal was oriented using the Laue back reflection technique to $\pm 1^\circ$. Optically clean portions of crystal were chosen and cut to $\sim 2 \times 2 \times 5$ mm$^3$ with long axis parallel to $\langle 100 \rangle$ and $\langle 110 \rangle$; both ends were polished with a diamond slurry down to 0.3 $\mu$m. Although optically clean portions were chosen in this study, TEM analysis revealed numerous precipitates (see later sections) that may affect plastic flow properties. Therefore, we have also performed deformation experiments after annealing to investigate the effects of precipitates in more detail.

Deformation experiments were made using a servo-controlled deformation apparatus in air. The apparatus is equipped with a $MoSi_2$ furnace and the temperature is controlled to $\pm 1$ K during an experiment. The compression direction was either along the $\langle 100 \rangle$ or the $\langle 110 \rangle$ axis. The pistons are made of SiC and no appreciable deformation of the pistons was detected under the present experimental conditions. In order to avoid chemical reactions between pistons and samples, thin discs of corundum were inserted between sample and pistons. Deformation experiments were performed in either a constant strain-rate or constant stress mode. However, in some experiments, strain-rate or temperature was changed during a single run to determine the stress exponent or activation energy. In these cases, each increment of experiment at a constant strain-rate or temperature was conducted until nearly steady state was reached.

After an experiment, thin sections were prepared by first mechanically grinding to ~20 micron thick followed by ion milling at 5 kV. The TEM observations were carried out at 200 kV with a JEOL 200CX microscope or at 300 kV with a PHILIPS CM30 microscope. We chose four samples for TEM analysis for which deformation experiments at constant stress were performed to ~10% strain.

As already noticed by several authors, characterisation of dislocation Burgers vectors is difficult in the garnet structure [5, 7, 8]. The reason is the large unit cell, which renders satisfactory two-beam diffraction conditions difficult to obtain. It is thus delicate to use the conventional method of characterisation based on the $\mathbf{g} \cdot \mathbf{b} = 0$ and $\mathbf{g} \cdot \mathbf{b} \times \mathbf{u} = 0$ invisibility criteria. Indeed, Ando *et al.* [7] chose an alternative method, based on the Burgers circuit, using high-resolution electron microscopy (HRTEM). In the present study, we have analysed the dislocations by large angle convergent beam electron diffraction: LACBED [9–11].

Let us recall briefly the principles of Burgers vector characterisation by LACBED. In this mode, when a dislocation intersects a Bragg line (i.e., the line where the exact Bragg condition is satisfied) with the diffraction vector **g**, the line rotates and splits into n nodes if $\mathbf{g} \cdot \mathbf{b} = n$ (Cherns and Preston rule; [9]). If the dislocation line is long enough, then it is possible to place it with respect to the Bragg lines so that it crosses at least three Bragg lines. Three linear equations of the type $g_i b = n_i$ are obtained whose solution uniquely gives the Burgers vector. If the dislocation is too short, then it is successively placed on three Bragg lines and the Burgers vector is deduced as above. This method requires knowledge of:

(i) $n$, the number of intensity minima in a dark field pattern.

(ii) the direction of the dislocation line characterised by a unit vector, **u**.

(iii) the *hkl* indices of the *Bragg* line.

(iv) the direction of the deviation parameter, s.

The last two features are identified by comparisons with theoretical patterns drawn by means of a computer program "Electron Diffraction" based on the kinematic theory which was developed by J. P. Morniroli (University of Lille) for this application. It is also possible to determine the direction **u** of the dislocation line by LACBED. One has to find (at least) two Bragg lines *hkl* and $h'k'l'$ which are parallel to the dislocation line. The unit vector **u** is then perpendicular to the corresponding **g** and $\mathbf{g}'$ vectors. This implies that **u** belongs to the planes *hkl* and $h'k'l'$. **u** is given by the intersection of these two planes (cross product $\mathbf{g} \times \mathbf{g}'$). The knowledge of the direction of the Burgers vector **b** and of the line direction **u** gives the glide plane of dislocation provided that the dislocation is not screw in character.

## 3. Results

### 3.1. Mechanical data

All the results of deformation experiments are summarised in Table I. Typical stress-strain curves for orientation [100] and [110] are shown in Fig. 1A and B respectively. They are characterised by initial elastic or work hardening stage followed by nearly steady state behaviour. The creep curves show a significant strain softening (see an example on Fig. 1C).

The steady state mechanical data are analysed assuming the power-law creep behaviour, viz.

$$\dot{\varepsilon} = A\sigma^n \exp(-E^*/RT) \qquad (1)$$

TABLE I Summary of creep results at steady state

| Run # | $T$(K) | $\dot{\varepsilon}$ ($10^{-6}$ s$^{-1}$) | $\sigma$ (MPa) | Orientation |
|---|---|---|---|---|
| CGGGD1-1[a] | 1522 | 2 | 221 | [100] |
| CGGGD1-2[a] | 1522 | 4 | 284 | [100] |
| CGGGD1-3[a] | 1522 | 8 | 346 | [100] |
| CGGGD2-1[a] | 1523 | 2 | 223 | [110] |
| CGGGD2-2[a] | 1523 | 4 | 289 | [110] |
| CGGGD2-3[a] | 1523 | 8 | 347 | [110] |
| CGGGD3-1[a] | 1472 | 4 | 386 | [100] |
| CGGGD3-2[a] | 1568 | 4 | 225 | [100] |
| CGGGD4-1[a] | 1472 | 4 | 404 | [110] |
| CGGGD4-2[a] | 1572 | 4 | 226 | [110] |
| CGGGD5 | 1573 | 4 | 200 | [100] |
| CGGGD6 | 1573 | 1.3 | 173 | [110] |
| CGGGD7 | 1573 | 5.8 | 170 | [100] |
| CGGGD8 | 1573 | 0.76 | 170 | [110] |

[a] Constant strain-rate tests.

where $\dot{\varepsilon}$ is strain-rate, $A$ is constant, $n$ is stress exponent, $E^*$ is activation energy, $R$ is the gas constant and $T$ is temperature. The stress exponent and the activation energy were determined by the step-wise tests where strain-rate or temperature was changed during a single experiment (Figs 1A, 2A and B). The compression direction appears to have only small effects on plastic flow properties. The difference in strengths of samples compressed along different orientations is indistinguishable and the flow law parameters such as the stress exponent and the activation energy are similar between the two. The linear regression yields $n = 3.1 \pm 0.3$, $E^* = 333 \pm 17$ kJ/mol.

## 3.2. TEM observations

### *3.2.1. The starting material*

The starting material is characterised by numerous tiny contrasts which appear on the background (Fig. 3). They appear either as black or white dots or exhibit a butterfly shape with a white and a black wing separated by a line of no contrast. These contrasts are typical of lattice strain effects around spherical precipitates [12]. The precipitates are distributed homogeneously in the sample and their size is less than 15 nm. We observed no dislocations in the starting material.

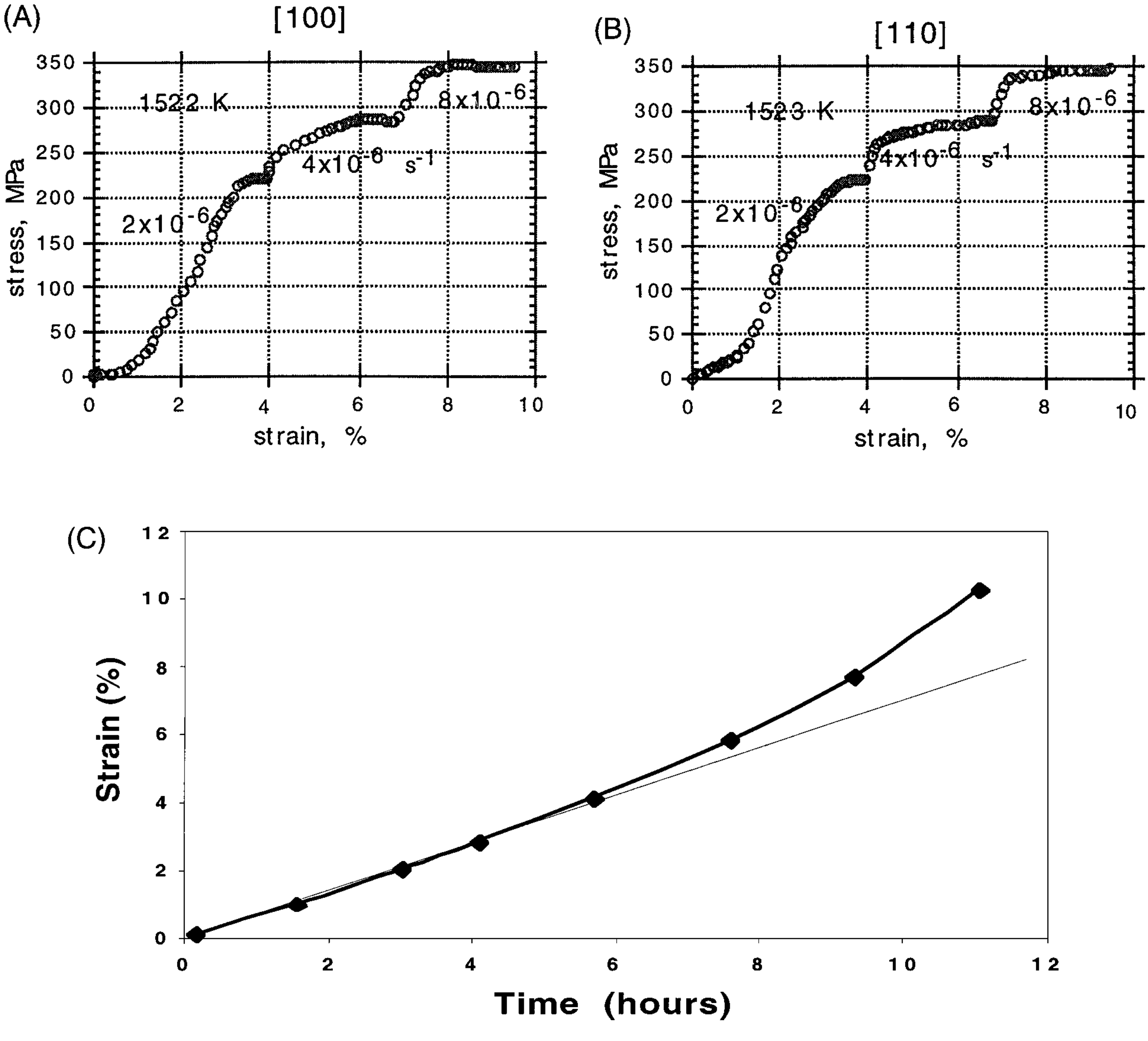

*Figure 1* Typical stress-strain curves: (A) a stress-strain curve for the [100] orientation; (B) a stress-strain curve for the [110] orientation and (C) a creep curve for [100] orientation.

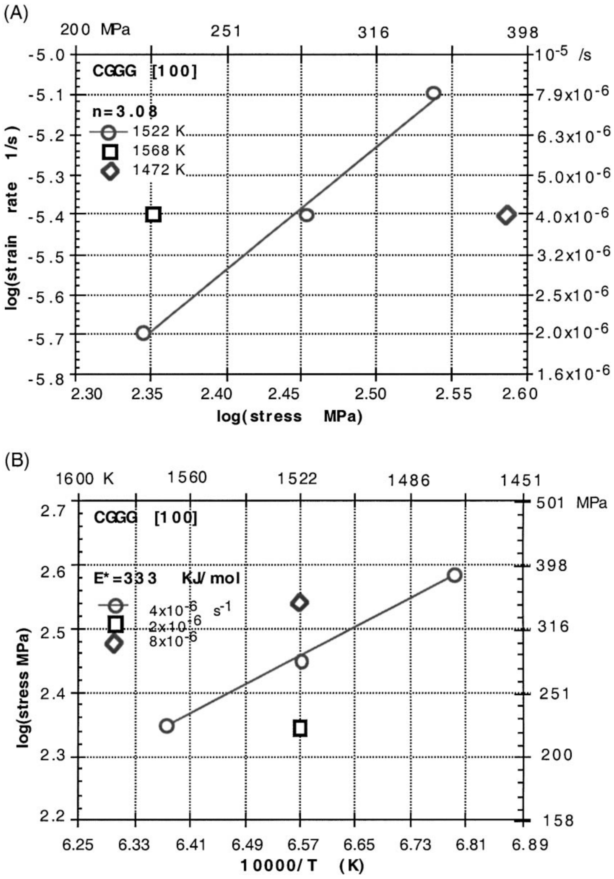

*Figure 2* Results of stress step tests (A) and temperature step tests (B) to determine the stress exponent and activation energy respectively.

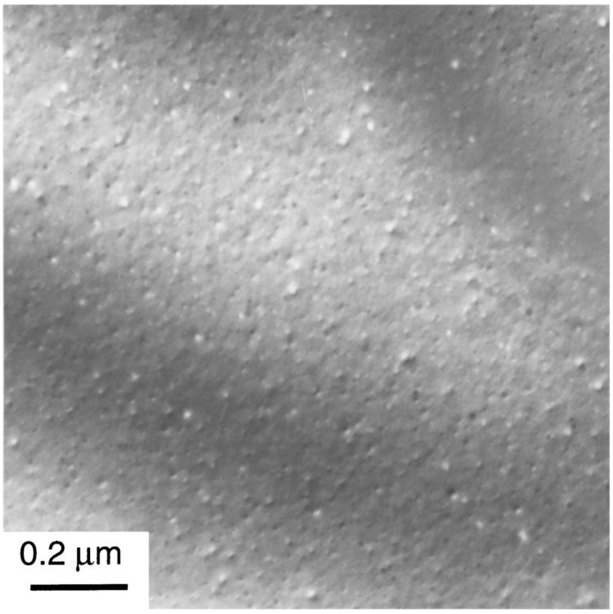

*Figure 3* Fine precipitation in the starting material. Bright field TEM micrograph. g: 400.

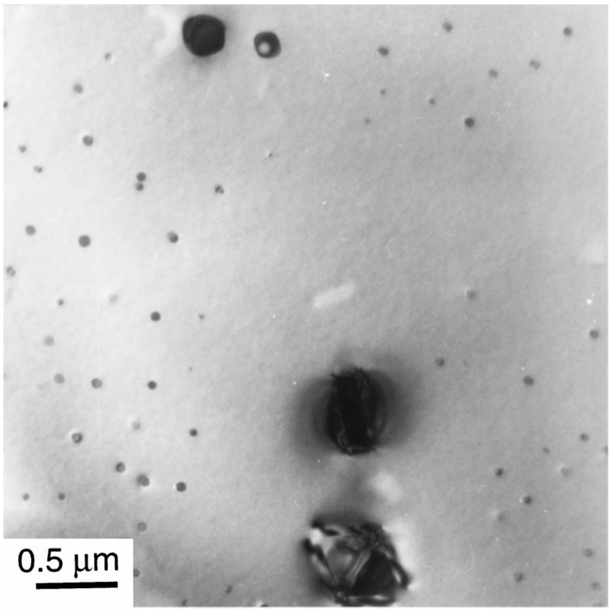

*Figure 4* 15 h annealed sample showing two kinds of precipitates. Bright field micrograph. g: 400.

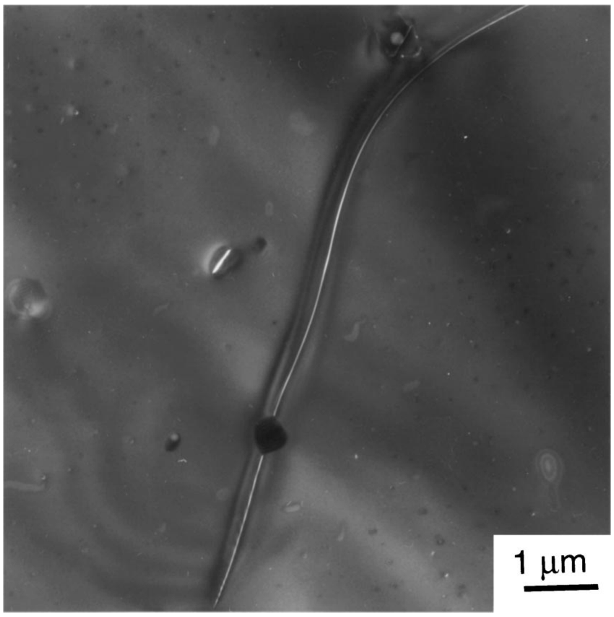

*Figure 5* 15 h annealed sample. Long dislocation segment lying in the foil plane {110}. Weak-beam dark field micrograph. g: 400.

### 3.2.2. Annealing experiments

Some samples have been annealed at 1573 K for 15 and 144 h before deformation experiments. After 15 h annealing, a significant evolution of the microstructure is noted (Fig. 4). The precipitates grew in size and the number density decreased. The precipitates seem to induce little or no elastic strain in the surrounding matrix. The distribution is more heterogeneous than in the starting material. Some areas are free from precipitates, whereas in other areas the number density reaches $\sim 5 \times 10^{19}$ m$^{-3}$. Typical size of precipitates is $\sim$0.05–0.08 $\mu$m whereas some larger ones (diameter $\sim$0.2–0.7 $\mu$m) are also observed. Their number density is $\sim 10^{17}$–$10^{18}$ m$^{-3}$. Finally, one observes dislocations connected to precipitates (Fig. 5). The dislocation density is heterogeneous and is in the range of $\sim 10^{9}$–$10^{11}$ m$^{-2}$. Annealing for 144 h changed the microstructure only slightly. The size and distribution of precipitates are similar to the sample annealed for 15 h at an identical temperature ($T = 1573$ K).

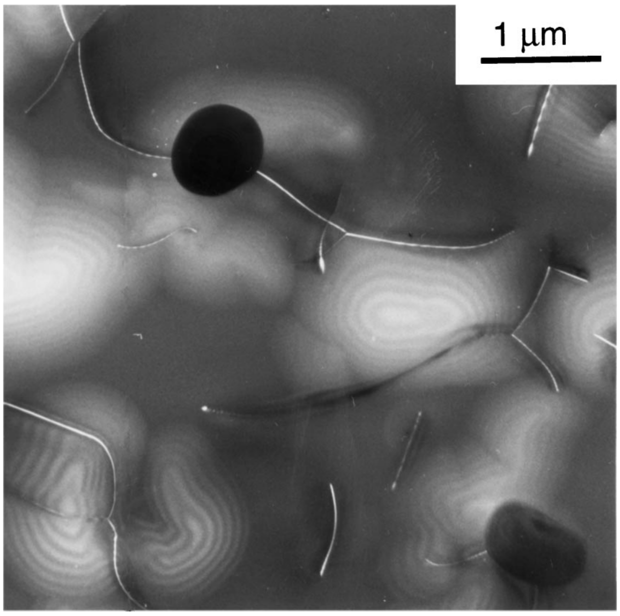

*Figure 6* CGGGD5 sample. Precipitates and dislocations. Weak-beam dark field micrograph. g: 400.

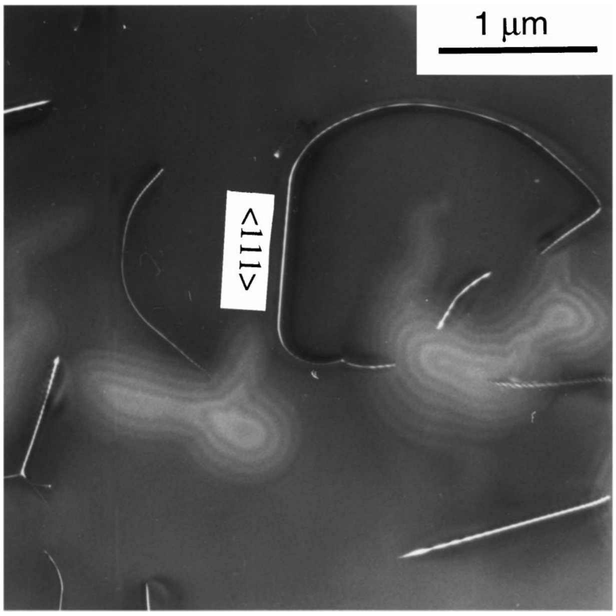

*Figure 8* CGGGD5 sample. Dislocation loop in a foil parallel to {110}. Weak-beam dark field micrograph. g: 400.

### *3.2.3. Deformed samples*

The samples CGGGD5 and CGGGD6 (hereafter referred to D5 and D6 respectively) have very similar microstructures. They will be described together.

One first note that the size of the precipitates increased and their number density decreased (Fig. 6). Their density is $\sim 10^{17}$–$10^{18}$ $m^{-3}$ and their size is $\sim 0.1$–1 $\mu$m. Dislocation distribution is homogeneous. The dislocation density is $\sim 10^{12}$ $m^{-2}$. In TEM foils prepared parallel to the creep specimen faces (i.e. in {001} planes containing the compression direction), the dislocations appear as short segments often involved in dislocation junctions (Fig. 7). No subgrain boundaries were observed in these samples. Numerous dislocations are interacting with precipitates (Fig. 6). Careful weak-beam, dark-field observations could not provide evidence of dislocation dissociation. Given that the resolution of the weak-beam imaging mode is approximately 10 nm in our case (see reference [13] for a discussion of the resolution in weak-beam), we conclude that the dislocations are either not dissociated or that the dissociation width is less than 10 nm.

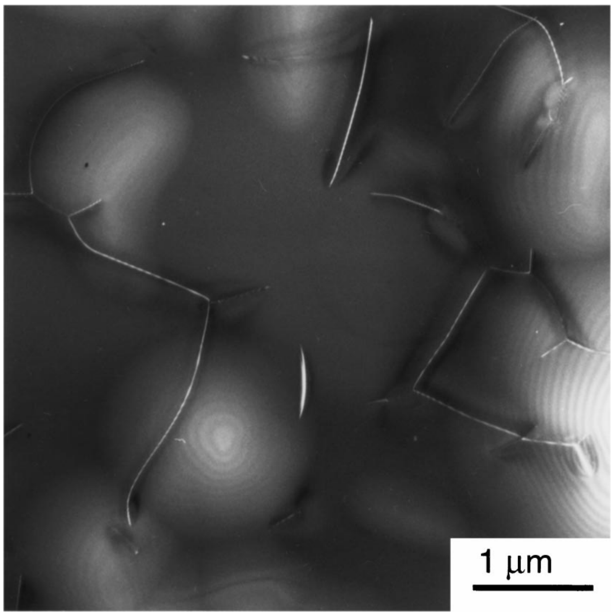

*Figure 7* CGGGD5 sample. Dislocation tangles. Weak-beam dark field micrograph. g: 400.

In sample D5, strained along $\langle 100\rangle$, two TEM thin foils have been cut parallel to two planes: a {110} plane (with a high resolved shear stress) and a {111} plane (a pure climb plane). The deformation microstructure in {111} is very similar to the one described above. There is no clear evidence that some dislocation lines belong to this plane. In contrast, one finds longer segments or dislocation loops in the {110} plane (Fig. 8). Some dislocation segments have marked crystallographic orientations: see for instance the segment oriented along $\langle 111\rangle$ on Fig. 8.

Dislocation Burgers vectors have been analysed by LACBED. Both $1/2\langle 111\rangle$ and $\langle 100\rangle$ dislocations can be found in both samples. However, $\langle 100\rangle$ dislocations can be formed in the garnet structure through attractive reactions such as $1/2[11\bar{1}] + 1/2[1\bar{1}1] = [100]$. We have thus taken a special care to avoid such reaction products. Only long dislocation segments that were (apparently) not involved in forming junctions were selected for Burgers vector analysis. With this criteria only $1/2\langle 111\rangle$ dislocations were found (22 dislocations in D5 and 10 dislocations in D6).

### *3.2.4. Samples deformed after annealing (CGGGD7, CGGGD8)*

As in the previous case, one finds numerous precipitates in the deformed samples. The size of the precipitates is similar to those in annealed samples. As in the previous section, the microstructures are very similar between D7 and D8. Some dislocations still present evidence of interaction with precipitates. Some precipitates are

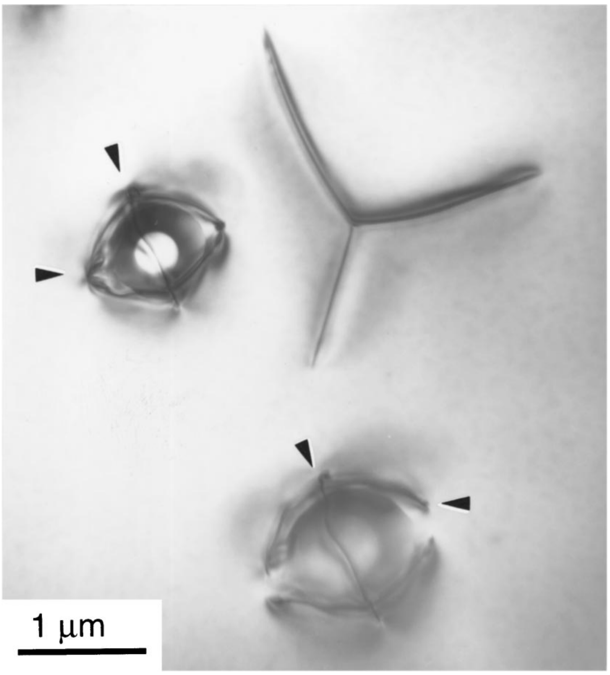

*Figure 9* CGGGD7 sample. Foil parallel to {110}. Precipitates enclosed by two (≈perpendicular) dislocation loops (arrowed). Bright field micrograph. g: 400.

enclosed by one or two (∼perpendicular) dislocation loops (Fig. 9). The most stringent difference between samples D5, D6 and D7, D8 is the much smaller dislocation densities (∼$10^{11}$ $m^{-2}$) in samples D7 and D8 than in D5 and D6. Similar to D5 and D6, no subgrain boundaries were observed. The dislocations show no evidence for dissociation in weak-beam dark-field.

As for D5, we have cut foils parallel to the {110} plane. We have observed long dislocation segments (Fig. 10) and loops which seems to lie in the foil plane.

LACBED characterisation of the Burgers vectors have been made following the same procedure as previously discussed (see an example of LACBED characterisation of a dislocation on Fig. 11). Again, only 1/2⟨111⟩ dislocations have been identified (7 in D7 and 2 in D8). The occurrence of several straight dislocations has allowed us to characterise, on the same dislocation, the line of direction and the Burgers vectors. The results are summarised in Table II. All these dislocations have a marked (in most cases pure) edge character. We have determined the following slip systems: 1/2⟨111⟩{110}, 1/2⟨111⟩{112} and possibly 1/2⟨111⟩{123}.

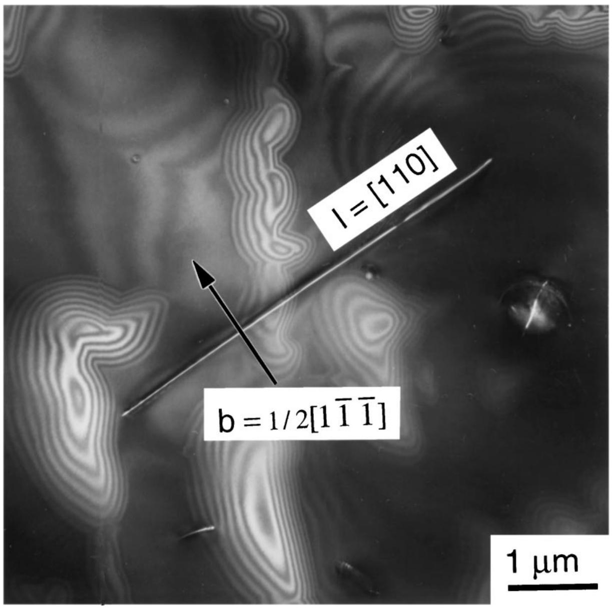

*Figure 10* CGGGD7 sample. Straight long dislocation segment in a foil parallel to {110}. Weak-beam dark field micrograph. g: 400.

TABLE II Burgers vectors (**b**) and dislocation line orientation (**l**) identified by LACBED in deformed $Ca_3Ga_2Ge_3O_{12}$

| Sample | Compression axis | **b** | **l** | $\alpha$ (°)[a] | Glide plane |
|---|---|---|---|---|---|
| CGGGD7 | ⟨100⟩ | (1/2)[$\bar{1}\bar{1}\bar{1}$] | [$\bar{1}1\bar{2}$] | 90 | (110) |
| CGGGD7 | ⟨100⟩ | (1/2)[$1\bar{1}\bar{1}$] | [110] | 90 | ($\bar{1}1\bar{2}$) |
| CGGGD7 | ⟨100⟩ | (1/2)[$\bar{1}11$] | [110] | 90 | ($\bar{1}1\bar{2}$) |
| CGGGD7 | ⟨100⟩ | (1/2)[$\bar{1}11$] | Compatible | | |
| | | | with [$1\bar{1}0$] | 144.7 | (110) |
| | | | and [$11\bar{1}$] | 109.4 | (101) |
| CGGGD7 | ⟨100⟩ | (1/2)[$1\bar{1}\bar{1}$] | Compatible | | |
| | | | with [112] | 118.1 | ($\bar{1}\bar{3}2$) |
| | | | and [113] | 121.5 | ($\bar{1}\bar{2}1$) |
| CGGGD8 | ⟨110⟩ | (1/2)[111] | [$\bar{1}1\bar{1}$] | 109.5 | ($\bar{1}01$) |
| CGGGD8 | ⟨110⟩ | (1/2)[$\bar{1}\bar{1}1$] | [$1\bar{1}1$] | 70.5 | ($0\bar{1}\bar{1}$) |

[a] Angle between **b** and **l**.

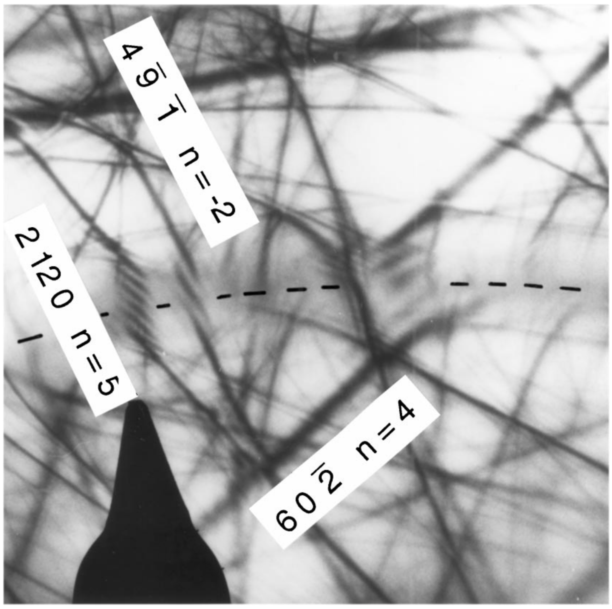

*Figure 11* LACBED analysis of Burgers vector dislocation: case of 1/2[$\bar{1}11$] dislocation (dotted line) crossed with 4 $\bar{9}$ $\bar{1}$, 2 12 0 and 6 0 $\bar{2}$ Bragg lines.

## 4. Discussion

### 4.1. Deformation mechanisms

The observed microstructures clearly point to dislocation glide as the operative deformation mechanism. We have many evidences from LACBED analysis or by direct observation of foils cut parallel to the expected glide planes that dislocations are gliding within those planes. Moreover, many dislocations have marked

TABLE III Schmid factors of typical slip systems for two compression axes

| Compression axis | Potential glide planes {*hkl*} | Schmid factor for ⟨111⟩ {*hkl*} | Experimentally observed glide planes |
|---|---|---|---|
| ⟨100⟩ | 110 | 0.41 | (110) (101) |
|  | 112 | 0.47 | $(\bar{1}1\bar{2})$ $(\bar{1}\bar{2}1)$ |
|  | 123 | 0.46 | $(\bar{1}\bar{3}2)$ |
| ⟨110⟩ | 110 | 0.41 | $(\bar{1}01)$ $(0\bar{1}\bar{1})$ |
|  | 112 | 0.47 |  |
|  | 123 | 0.46 |  |

crystallographic orientations, which indicates that they bear high lattice friction.

Dislocation Burgers vector analysis shows that $\mathbf{b} = 1/2\langle 111\rangle$ has been activated in all samples. The case for $\mathbf{b} = \langle 100\rangle$ dislocations is somewhat more delicate because they can be formed by a reaction among $\mathbf{b} = 1/2\langle 111\rangle$ dislocations. Therefore these dislocations can be observed in any samples. However, we found no clear evidence suggesting that ⟨100⟩ dislocations contribute significantly to plastic deformation in any of our samples, although this conclusion can not be definitive. The 1/2⟨111⟩{110} appears to be the most frequently observed slip system (Table II) although it has slightly lower Schmid factor than the 1/2⟨111⟩{112} or the 1/2⟨111⟩{123} slip systems (Table III). This result is in good agreement with most of previous studies on 3-3 oxide garnets [1, 14] or 2-3-4 silicate garnets either experimentally [15, 16] or naturally deformed [17].

It is remarkable, given the high temperature of the deformation experiments (∼0.95 $T_m$) to observe that dislocation motion is restricted to their glide planes and many dislocation segments are straight. This indicates that the dislocations experience high lattice friction. Some of these stable dislocation lines have been characterised here by LACBED. (Table II). One notes that all the analysed dislocations have a significant edge character (some are even pure edge dislocations) even those along the ⟨111⟩ direction. No screw dislocations were found in contrast with bcc metals and previous studies on 3-3 oxide garnets (e.g. [1]). These particular dislocation structures probably reflect some fine structure of the dislocation core. It is likely that the core of dislocations in garnets is extended and non-planar. No dissociation could be identified however with weak-beam dark field observations.

Another puzzling observations is the absence of subboundaries. Although the absence of subboundaries in 3-3 garnets was noted by some previous studies [4, 14], numerous subboundaries are often found in many previous studies in garnets including some on synthetic 3-3 garnets [1, 18] or naturally deformed 2-3-4 garnets [7, 8, 15, 16, 19–21]. Possible causes for this discrepancy include the differences in strain magnitudes and/or the degree of strain homogeneity, but the exact reason for this discrepancy is not well understood.

## 4.2. Precipitates-dislocations interaction

The TEM investigations first revealed that the starting material contains some tiny precipitates (<15 nm). Characterisation of deformed samples D5 and D6 shows that these precipitates grew and/or coarsened as the samples were deformed. Annealing experiments without stress also resulted in similar effects. Precipitates similar to the ones observed in our annealed or deformed samples were reported in CGGG [22]. These authors interpreted the precipitates as being Ga-rich and Ge-depleted materials within the garnet structure resulting from evaporative loss of Ge during growth [22].

There are microstructural evidence that dislocations interact with precipitates (Figs 6 and 9). This is supported by the observation that dislocation densities in D7 and D8 is smaller than those in D5 and D6 which were deformed at similar stress levels. However, the nature and strength of this interaction is not clear from the observed microstructures. In particular, it is not clear whether the precipitates are sheared by the dislocations (Fig. 6 could be interpreted along this line) or by-passed by an Orowan mechanism. The latter mechanism would be suggested by the dislocation loops observed around some precipitates (Fig. 9). For the Orowan mechanism, the hardening induced by the precipitates is given by $\Delta\sigma \sim \mu b/L$ where $\mu$ is the shear modulus (∼90 GPa), $b$ is the length of the Burgers vector (∼1 nm) and $L$ is the mean spacing between precipitates. Our microstructural observations show that in the starting material, $L$ can be as small as 50 nm. The hardening resulting from an Orowan interaction would be very large, at least at the beginning of the deformation experiments. Deformation being accompanied by precipitates coarsening; one would expect a very large softening during deformation. We do observe a softening effect, but this effect is moderate. Moreover, the mechanical results show that the differences in creep behaviour between unannealed and annealed samples are small. Therefore, we conclude that the interaction between dislocations and precipitates is small.

## 4.3. Comparison with other garnets

The present results have shown large similarities in deformation behaviour between $Ca_3Ga_2Ge_3O_{12}$ and oxide garnets studied previously [1, 4, 14]. Common to other garnets, $Ca_3Ga_2Ge_3O_{12}$ has very high strength even at high homologous temperatures (Fig. 12). The stress exponent ($n \sim 3$) is similar to other garnets and is consistent with the glide controlled mechanism(s) of creep [23]. This is in agreement with our TEM observations which indicate absence of dislocation climb and with the previous mechanical results which showed a small internal stress [4, 14].

However, there are some differences between $Ca_3Ga_2Ge_3O_{12}$ and other 3-3 garnets. The most notable is the observation that dislocations with large edge component dominates the microstructure in $Ca_3Ga_2Ge_3O_{12}$ whereas it is dominated by screws in other 3-3 garnets. The dominance of screws is well documented in bcc metals. The three-fold symmetry of a screw dislocation aligned along a ⟨111⟩ direction results in a sessile splitting of the core on several planes ({110} and possibly {112}). This sessile configuration is responsible

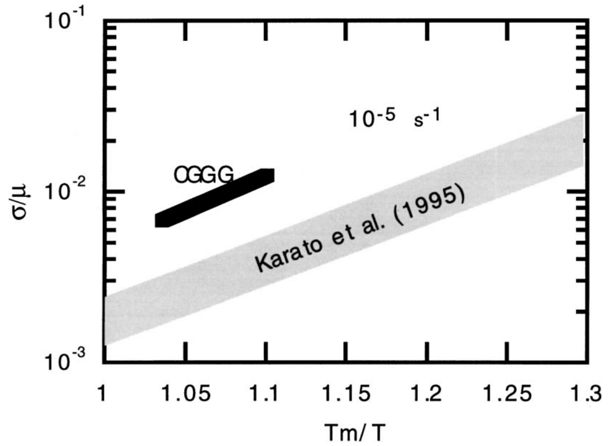

*Figure 12* Comparison of the present results on CGGG with other garnets reported by Karato *et al*. [4]. The comparison is made at the strain-rate of $10^{-5}$ $s^{-1}$. $T$: temperature, $T_m$: melting temperature, $\mu$: shear modulus, $\sigma$: creep strength. The results are largely consistent with the results of other garnets, although the normalised creep strength of CGGG is considerably larger than those of other garnets.

for a high Peierls stress, the screw dislocation motion being a sequence of sessile-glissile-sessile transformations. The deformation of garnets, which belong to the same bcc Bravais lattice, has been described following the same lines. However, Rabier *et al*. [5] have pointed out the effect of the crystal chemistry of the garnets on the possible dissociation of the dislocations. They have looked for the planar defects that leave the most dense cation sublattice (the one of the octahedral cations) unaffected. They have shown in particular that some stacking faults (involving a displacement $1/4\langle 111\rangle$) yield to a great increase in electrostatic energy while some others (displacements $1/2\langle 100\rangle$ or $1/2\langle 110\rangle$) lead, in 3-3 garnets, to a less expensive order fault as they exchange two different ion sites which carry the same charge (3+). These planar defects are called Electrostatic Fault (EF) and Order Fault (OF) respectively. It is likely that in 3-3 garnets the dislocation core of the screw dislocations involves such energetically favourable (OF) stacking fault components. In the case of 2-3-4 garnets, the displacements $1/2\langle 100\rangle$ or $1/2\langle 110\rangle$ will also be associated with a change in the electrostatic energy. It is thus expected that the dislocation core of 3-3 and 2-3-4 garnets will have a different fine structure. Indeed, it is shown that in 3-3 garnets as well as in bcc metals, the dislocations with the lower mobility (i.e. dislocations with the more stable core configuration) are the screw dislocations [1]. These low mobility dislocations thus dominate the deformation microstructure observed in the TEM. In contrast, the present study emphasises the fact that the dislocations that bear the stronger lattice friction are not screws. The more stable configuration still involves a dislocation line aligned with a $\langle 111\rangle$ direction, but the Burgers vectors corresponds to a different $\langle 111\rangle$ vector: for instance $1/2[111]$ aligned along $[\bar{1}\,1\,\bar{1}]$ (see Table II). The same characteristic dislocations (couple dislocation Burgers vector and dislocation line) are found in silicate garnets either experimentally or naturally deformed [16, 17]. It is to be remembered that garnets are almost perfectly isotropic from the elastic point of view (in crystals with the cubic symmetry, elastic anisotropy is usually estimated from the deviation from unity of the quantity $2C_{44}/(C_{11}\text{-}C_{12})$; in garnets, this quantity varies slightly with composition, but it remains very close to unity). The dislocation segmentation cannot be attributed to an effect of anisotropy and must reflect the structure of the dislocation core. The dislocation structure (core configuration) thus appears to be different in 3-3 garnets and in 2-3-4 garnets. From that respect, $Ca_3Ga_2Ge_3O_{12}$ appears to be a better analogue to silicate garnets for deformation studies.

## 5. Conclusions

High temperature deformation of single crystal $Ca_3Ga_2Ge_3O_{12}$ has been experimentally investigated. $1/2\langle 111\rangle\{110\}$ appears to be the easy slip system. The mechanical data showed that $Ca_3Ga_2Ge_3O_{12}$ garnets have a high resistance to creep similar to other 3-3 garnets. This is interpreted on the basis of TEM observation as being the result of a high resistance to dislocation glide (high Peierls stress). The dislocation core structures appear to be more similar to silicate garnets (which also have 2-3-4 cation charges) than to other 3-3 synthetic garnets. In particular, the most stable dislocations are not the screws as in 3-3 garnets (or bcc metals) but dislocations with a large edge component. This is interpreted as resulting from different dissociations in the dislocation core. These dissociations cannot be seen with the TEM however.

## References

1. J. RABIER and H. GAREM, in "Deformation of Ceramic Materials II," edited by R. E. Tressler and R. C. Bradt (Plenum Press, New York, 1984) p. 187.
2. A. E. RINGWOOD, *Geochim. Cosmochim. Acta* **55** (1991) 2083.
3. M. AKAOGI and S. AKIMOTO, *Phys. Earth Planet. Inter.* **15** (1977) 90.
4. S. KARATO, Z. WANG, B. LIU and K. FUJINO, *Earth Planet. Sci. Lett.* **130** (1995) 13.
5. J. RABIER, P. VEYSSIERE and J. GRILHE, *Phys. Stat. Sol. (a)* **35** (1976) 259.
6. P. PAN, T. YAMAZAKI, A. SUGIMOTO, K. YAMAZAKI and H. TAKEI, *Jpn. J. Appl. Phys.* **34** (1995) 515.
7. J. ANDO, K. FUJINO and T. TAKESHITA, *Phys. Earth Planet. Inter.* **80** (1993) 105.
8. N. DOUKHAN, V. SAUTTER and J.-C. DOUKHAN, *ibid.* **82** (1994) 195.
9. D. CHERNS and A. R. PRESTON, in Proceedings of Eleventh International Congress on Electron Microscopy (Kyoto, 1986) Vol. 1, p. 721.
10. M. TANAKA, R. SAITO, K. UENO and Y. HARADA, *J. Electron Microscopy* **29** (1980) 408.
11. D. CHERNS and J. P. MORNIROLI, *Ultramicroscopy* **53** (1994) 167.
12. M. F. ASHBY and L. M. BROWN, *Phil. Mag.* **8** (1963) 1083 and 1649.
13. M. SARIKAYA and J. M. HOWE, *Ultramicroscopy* **47** (1992) 145.
14. Z. WANG, S. KARATO and K. FUJINO, *Phys. Chem. Mineral.* **23** (1996) 73.
15. P. CORDIER, P. RATERRON and Y. WANG, *Phys. Earth Planet. Inter.* **97** (1996) 121.
16. V. VOEGELE, J. ANDO, P. CORDIER and R. C. LIEBERMANN, *ibid.* **108** (1998) 305.

17. V. VOEGELE, P. CORDIER, V. SAUTTER, T. G. SHARP, J. M. LARDEAUX and F. O. MARQUES, *ibid.* **108** (1998) 319.
18. J. RABIER, P. VEYSSIERE, H. GAREM and J. GRILHE, *Philos. Mag.* **39** (1979) 693.
19. H. CARSTENS, *Contr. Mineral. Petrol.* **24** (1969) 348.
20. S. JI and J. MARTIGNOLE, *Journal of Structural Geology* **16** (1994) 985.
21. J. CHEN, Q. WANG, M. ZHAI and K. YE, *Science in China (D)* **39** (1996) 18.
22. T. F. ROTH, R. K. MISHRA and G. THOMAS, *J. Appl. Phys.* **52** (1981) 219.
23. H. J. FROST and M. F. ASHBY, “Deformation Mechanism Maps” (Pergamon Press, Oxford, 1982) p. 167.

*Received 17 February 1998*
*and accepted 26 March 1999*